https://doi.org/10.1016/j.compscitech.2022.109778

Localizing the cross-links distribution in elastomeric composites by tailoring the morphology of the curing activator

Silvia Mostoni [a], Paola Milana [a], Claudia Marano [b], Lucia Conzatti [c], Michele Mauri [d], Massimiliano D'Arienzo [a], Barbara Di Credico [a], Roberto Simonutti [d], Paola Stagnaro [c], Roberto Scotti [a*]

[a] *Department of Materials Science, INSTM, University of Milano Bicocca, Via Roberto Cozzi 55, 20125 Milano, Italy;* [b] *Department of Chemistry, Materials and Chemical Engineering "Giulio Natta", Politecnico di Milano, Piazza Leonardo Da Vinci 32, 20133 Milano, Italy;* [c] *Consiglio Nazionale delle Ricerche – Istituto di Scienze e Tecnologie Chimiche "G. Natta" (CNR-SCITEC) Via De Marini 6, 16149 Genova, Italy;* [d] *Department of Materials Science, University of Milano Bicocca, Via Roberto Cozzi 55, 20125 Milano, Italy.*

Abstract

In this work the localization of the rubber vulcanization reaction close to the silica filler surface was investigated in isoprene rubber composites (IR NCs) to highlight the role of both the curing agents' dispersion and the filler surface features on the spatial propagation of chemical cross-links between the rubber chains and the resulting mechanical behavior of the material. The study was realized by tailoring the morphology of the curing activator, i.e. by vulcanizing IR NCs with Zn@SiO_2 double function filler, composed of Zn(II) single sites anchored on SiO_2 filler, as curing activator, in comparison to silica filled IR NCs vulcanized with microcrystalline ZnO (m-ZnO). The microscopic cross-links distribution was measured by Transmission Electron Microscopy (TEM) and Time Domain Nuclear Magnetic Resonance (TD-NMR). Besides the NCs mechanical behavior was characterized both at small strain and at fracture. In the presence of Zn@SiO_2, the formation of a higher cross-link density in proximity to SiO_2 particles which gradually spreads from the surface to the bulk, induced by the localized active Zn(II) centers was evidenced. Further IR NCs material resulted stiffer and with a lower fracture toughness, with respect to m-ZnO based NCs, which

Corresponding author: Prof. Roberto Scotti
email: roberto.scotti@unimib.it
tel: +390264485133

shows a quite homogeneous structure of the polymer cross-links network in the rubber matrix. The results highlighted the correlation between the composites structural features and their macroscopic behavior, paving the way to modulating the mechanical properties by tuning the nature of the curing agents.

Keywords: nano composite (A); nano particles (A); interface (B); microstructure (B); mechanical properties (B)

1. Introduction

The mechanical properties of rubber nanocomposites (NCs), used for several material applications as tires, arise both from the use of reinforcing fillers as silica nanoparticles (NPs), silicate or carbon-based materials [1–3] and the formation of an extended polymer network through a curing process. The vulcanization is the industrial thermal process with sulfur (S_8) that converts the rubbery molecules into a three-dimensional network structure, inducing their covalent cross-linking [4,5], by formation of sulfur bridges between the polymer chains. Other curing agents, such as organic accelerators (i.e. sulfenamides, thiurams, etc.), activators (metal oxides as ZnO) and co-activators (i.e. fatty acids) are commonly added to rubber compound as well to improve processability, vulcanization rate, and cross-linking efficiency [6–8]. In fact, though the reaction mechanism is not completely understood, several authors state that ZnO and especially Zn(II) ions react with the accelerator and S_8 in the first reaction steps to form active sulfurating agents complexes [9–12], that boost the interaction of S_8 with rubber, reducing the reaction time and energy consumption. Besides, activators exert a remarkable impact on the structure of the vulcanized NCs [13], as intermediate Zn(II) complexes are supposed to further interact with the sulfur cross-links, promoting the shortening process of poly-sulfide chains, thus leading to mono- and di-sulfide bridges and consequently, more strongly cross-linked materials [14].

However, despite the long history of vulcanization, the control over the polymer network formation during the process is still an open issue, as it depends on several parameters including the distribution of the curing agents into the matrix during the mixing phase and their diffusion during the curing process [15–17]. In general, sulfur cured NCs are believed to present a not homogeneous distribution of the cross-links associated to an uneven dispersion of curing agents. Many authors [18–21] ascribed nonuniform cross-links' distribution to the presence of ZnO and ZnS aggregates (typical vulcanization by-product), by investigating different elastomers, such as styrene-butadiene rubber (SBR), natural rubber (NR) and butadiene rubber (BR), through morphological and spectroscopic analyses. This affects the nano-sized structure of cured NCs, as well as the elasticity and mobility of rubber chains.

Similar observations were recently reported by Ikeda et al. [22] who focused on the role of Zn-accelerating complexes claiming that nonuniform networks domains grow due to the adsorption of both sulfur and accelerator on residual ZnO aggregates, giving rise to localized cross-linking areas close to them and affecting the length of the sulfur chains as assessed by Atomic Force Microscopy based Young modulus measurements [23,24] and complementary NMR studies. Valentin et al. [25] highlighted that inhomogeneities in sulfur cured NCs can only be found at the micrometric scale, due to non-rubber components, especially in rubber blends [26]. Whereas a rather homogeneous rubber matrix was detected at more local nanometric scale through multiple quantum (MQ) excitation sequences NMR, showing only one component in the rubber cross-links' distribution.

Although all these studies have tried to give insights into the cross-links' distribution in vulcanized rubber NCs evidencing the role of curing agents in the network formation, far less attention has been dedicated to the reciprocal influence of cross-linking and filler networking into the rubber matrix. In fact, the properties of cured NCs are determined not only by the overall cross-links' organization in the rubber matrix but rather by their relative arrangement

in proximity to the filler surface and network, envisaging a critical role of the morphology and surface features of the filler NPs on the spatial propagation of chemical cross-link process. This aspect becomes even more relevant considering the possibility of using filler systems that behaves as a vulcanization activator and a reinforcing agent, simultaneously [27,28].

In this scenario, the present work aims at studying the chemical cross-linking process and the resulting mechanical properties of isoprene rubber (IR) NCs vulcanized in the presence of two morphologically different zinc-based activators. The conventional microcrystalline ZnO activator (m-ZnO), mixed with SiO_2 NPs as filler in the bulk rubber was herein compared to $Zn@SiO_2$ double function filler, constituted by Zn(II) single sites anchored on the surface of SiO_2 filler particles [27]. The choice of $Zn@SiO_2$ NPs lies in their high curing efficiency [28] and in the challenging possibility to localize the active sites triggering the cross-linking process close to SiO_2 NPs, thus inducing the network formation and propagation directly from the filler surface. The final purpose of this study is to demonstrate that the localization of the vulcanization reaction provides a change in the microscopic structure of the cross-linked polymer network in the vulcanized NCs and, consequently, different mechanical behavior of the material, achieving a fine control of both the micro- and macro-properties of the rubber products. The microstructures of the IR NCs were investigated through a multidisciplinary approach, which involves: i) swelling experiments, ii) a morphological study by using Transmission Electron Microscopy for network visualization (NVTEM) to investigate either filler network and IR network distribution, iii) Time Domain (TD) NMR analysis to assess the cross-linking degree of the high mobility rubber fraction in the cured NCs and to quantify the lower mobility polymer fractions related to rubber/filler interaction. Finally, the mechanical response of IR NCs was characterized both at small strains and at fracture, to highlight a correlation between microstructures and macroscopic properties.

2. Experimental

2.1 Materials

$Zn@SiO_2$ synthesis: precipitated silica Rhodia Zeosil MP1165 (BET specific surface area 160 $m^2\ g^{-1}$) was purchased from Rhodia; (3-aminopropyl) triethoxysilane ($(H_2N(CH_2)_3Si(OC_2H_5)_3$, 99%, APTES) from Sigma Aldrich; toluene (99%) and zinc nitrate hexahydrate $Zn(NO_3)_2{\cdot}6H_2O$ from Alfa Aesar; anhydrous ethanol EtOH (99.9%) from Exacta+Optech Labcenter.

Rubber compounding: IR was purchased from Nizhnekamskneftechim Expor; bis(3-triethoxysilylpropyl) disulfide (TESPD) from Aldrich; antioxidant *N*-(1,3-dimethylbutyl)-*N*'-phenyl-*p*-phenylenediamine, 6PPD Santoflex-6PPD from Flexsys; stearic acid (Stearina TP8, SA) from Undesa; *N*-cyclohexyl-2-benzothiazole sulfenamide (CBS) Vulkacit CZ/C from Lanxess; sulfur Creso (S_8) from Redball Superfine; m-ZnO, BET specific surface area 5 $m^2\ g^{-1}$) from Zincol Ossidi (wurtzite).

TEM analysis: styrene (99%, containing 10-15 ppm 4-*tert*-butylcatechol inhibitor), di-*n*-butyl phthalate (DBP, 99%) and Osmium tetroxide (OsO_4, ReagentPlus, 99.8%) were purchased from Sigma Aldrich and used as received. Benzoyl peroxide (BPO) 70% (stabilized with 30% water) was purchased from Aldrich, dried over P_2O_5 and then stored in a desiccator until use.

2.2 Preparation of $Zn@SiO_2$ and silica/IR NCs

$Zn@SiO_2$ was synthesized according to a two-step procedure previously described [27] and here summarized. In the first step, SiO_2 NPs were functionalized with APTES using a molar ratio between APTES and SiO_2 surface silanol groups (n_{APTES}/n_{OH}) equal to 1/2 (solvent toluene, 24 h, reflux conditions). Then, Zn(II) centers were loaded on the pre-functionalized SiO_2 with a Zn:APTES molar ratio (n_{Zn}/n_{APTES}) equal to 1/2 (ethanol, 2 h, 100 °C), so that each Zn(II) center interacts with two amino groups in a structure as shown in Figure S1 in the Supplementary Information (SI). The experimental conditions were set to obtain [27]: i)

APTES amount on SiO_2 equal to 7.6 wt% (corresponding to ~ 5 molecules nm^{-2} of SiO_2), ii) Zn loading in Zn@SiO_2 equal to 3.1 wt% (~ 2.5 Zn atoms nm^{-2} of SiO_2).

Zn@SiO_2/IR NCs were prepared by mixing IR with Zn@SiO_2 as filler and curing activator (48.1 parts per hundred rubber, phr) correspondent to SiO_2 = 43.0 phr and Zn = 1.5 phr). These NCs were compared to silica/IR NCs prepared using SiO_2 NPs as filler (43.0 phr) and m-ZnO as curing activator (1.8 phr, equal to Zn = 1.5 phr), herein called ZnO+SiO_2/IR.

For both Zn@SiO_2/IR and ZnO+SiO_2/IR NCs the ingredients were mixed in a Brabender Plasti-Corder lab station internal mixer (65 mL mixing chamber, 0.6 filling factor, 60 rpm rotor speed) following a conventional three-step procedure: i) IR was masticated into the mixing chamber and mixed with the filler and antioxidant 6-PPD (2.0 phr) at T = 90 °C for 3 min. In ZnO+SiO_2/IR, m-ZnO, SA (2.0 phr) and TESPD (3.2 phr) were further added at this step and the temperature was increased to 145°C, to assure the filler compatibilization; ii) IR NCs were reloaded into the mixing chamber and the accelerator CBS (1.6 phr) and S_8 (3.0 phr) added and mixed at T = 90 °C for 3 min; iii) IR NCs were further mixed at T = 50 °C, for 3 min in a two-rolling mill, to improve the uniform distribution of the additives.

Vulcanization reactions of IR NCs were performed using a Rubber Process Analyzer (RPA 2000, Alpha Technological) and monitored by measuring the torque values (S') over vulcanization time (vulcanization curves). RPA vulcanization conditions are: time = 5 min; T = 170 °C; frequency = 1.670 Hz; shear strain = 7 ± 1 %.

2.3 Characterization of silica/IR NCs

Swelling experiments in toluene were used to assess the cross-linking density (ν_{SW}) of IR NCs, according to the Flory-Rehner approach (Eqs. S1-S2). Samples (m_0 = 1.00 g ± 0.05 g) were swollen in fresh toluene (25 mL) for four days into closed vessels, changing toluene daily, and finally dried at room temperature (RT) for 24 h.

For the NVTEM, specimens of vulcanized IR NCs sheets were extracted overnight in refluxing $CHCl_3$ using a Soxhlet apparatus and then dried under vacuum. After the extraction, the samples were swollen to equilibrium in a styrene solution containing 2 wt% DBP and 1 wt% BPO for 4 days at RT. To ensure a complete swelling, samples were further heated at 40 °C for 5 h in excess styrene solution. Then, the styrene polymerization was carried out at 70 °C for 16 h and completed by raising the temperature up to 90 °C for 4 h. Ultrathin sections (about 50 nm thickness) for TEM analysis were obtained from NCs samples frozen at – 130 °C by using a LEICA EM FCS cryo-ultramicrotome equipped with a diamond knife. The sections were collected from different zones of each sample and placed on copper grids. TEM images were taken with a Zeiss EM 900 microscope operating at 80 kV on: i) pristine vulcanized sheets; ii) PS-swollen samples before staining; and iii) PS-swollen samples after staining with OsO_4 vapors. TEM images were obtained with a Zeiss EM 900 microscope operating at 80 kV. A schematic representation of the sample preparation before NVTEM analysis is reported in Figure 1.

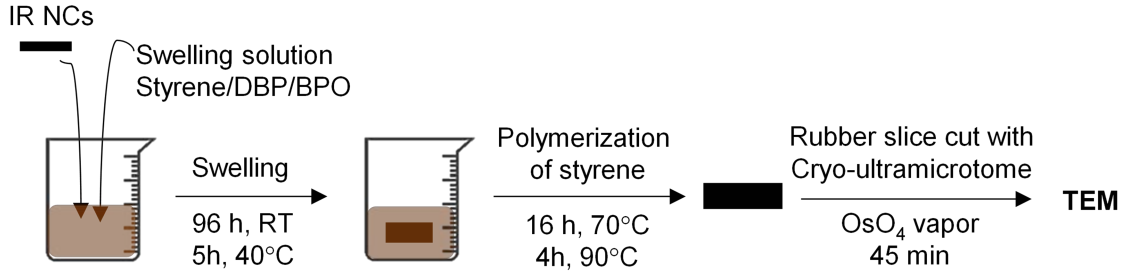

Figure 1. Representation of IR NCs swelling procedure with styrene for NVTEM analysis.

TD-NMR experiments were performed using a Bruker Minispec (ND series) operating at 20 MHz frequency. TD-NMR was used both to evaluate the cross-linking degree of the mobile fraction and to measure the rigid polymer fractions. For the cross-linking degree, the alternate acquisition of MQ and reference signals with a variant of the Baum-Pines sequence developed for benchtop instruments was performed, later improved with a randomization of the MQ excitation time sampling [29]. Experiments were repeated in triplicates to further

validate the results. The resulting double quantum (DQ) build-up curves were then corrected for the presence of dangling ends and polymer chains not connected to the network, and analyzed with the Tikhonov regularization using Abragam-like kernel function [30]. The resulting distribution of residual dipolar couplings (D_{res}) that can be used to distinguish fine details of the cross-linked structures. Besides, from average D_{res} values, the cross-linking densities (ν_{NMR}) of IR NCs were calculated and compared to the previous results of the swelling experiments (Eqs. S3-S4).

The measurement of the rigid rubber fraction was carried out by collecting free induction decay (FID) after performing a Magic Sandwich Echo (MSE) refocusing block [31].

Calorimetric properties of both vulcanized IR NCs were investigated by using a DSC-1 system (Mettler Toledo). Around 10 mg were used for each experiment and inserted in 40 μL Al crucibles with pierced lid. Experiments were performed as here reported: i) a first heating was carried out from -150 to 60 °C; ii) the samples were then cooled to -150 °C; iii) a second heating step up to 100 °C was finally performed. For each ramp, a heating rate of 20 °C min^{-1} was adopted and the whole experiment was made under a nitrogen flow (80 mL min^{-1}).

Dynamic-mechanical tests were performed, under uniaxial tensile loading conditions, using a TA RSA III Analyzer. Prismatic-specimens, having a cross section area of (4 x 2) mm^2 and a gauge length of 20 mm, were used. A static deformation (ε_s) was first applied, and a dynamic strain (ε_d) was then superimposed (the static strain was step-by-step increased from 0.05 to 300 %; the dynamic strain was applied at a frequency of 10 Hz, with an amplitude equal to 0.05 % of the actual specimen length). After each dynamic measurement, a stress relaxation period (about 30 s) was allowed before performing the following step of the dynamic test. The conservative component modulus E' of the material complex modulus was evaluated for each value of the applied static deformation, ε_s.

Uniaxial tensile tests were performed by using a Hounsfield dynamometer equipped with a 5 kN cell and with a mechanical extensometer necessary for the measurement of dumb-bell shaped specimen elongation in its gauge length. A pneumatic system was used to clamp the specimen. Specimens having 2 mm of thickness and an initial gauge width and length of 4 and 20 mm respectively were used. A displacement rate of 50 mm min^{-1} was applied, corresponding to a nominal strain rate $\dot{\varepsilon}$ = 3.57 min^{-1}. From the stress strain curves, the Mooney Rivlin plots were obtained following Eqs. S5-S6.

Fracture tests were carried out using large and short strip-shaped specimens, which are usually referred to as pure shear specimens. An edge notch, with a length a = 22 mm, was introduced with a razor blade, just before the test. The tests were performed on an Instron screw-driven dynamometer equipped with a 10 kN load cell at a constant displacement rate of 50 mm min^{-1}. The tests were video recorded to evaluate the time of crack initiation and to observe the fracture phenomenology. From the load-displacement curve the energy to fracture onset, U_i, was measured and used to evaluate the material fracture toughness, following Eq. S7. This equation reports the analytical expression, valid for the adopted specimen-geometry, of the so-called *J*-integral, which is the variation of elastic energy stored in the material per unit area of crack: the value of the J integral at crack onset, Jc, is used to analyze the fracture behavior of nonlinear elastic solids like rubbers [32].

3. Results

IR NCs were compounded and cured by using Zn@SiO_2 as double function filler, behaving both as reinforcing filler and curing activator, and compared with IR NCs where m-ZnO and bare SiO_2 NPs were used as activator and filler, respectively. The vulcanization curves by RPA demonstrate in both processes the effective sulfur cross-link formation, showing the increase of the torque (S') over time (Figure S2). The higher maximum S', along with the lower optimum curing time further evidenced the higher vulcanization efficiency in the

presence of Zn@SiO_2, confirmed also by the higher cross-linking densities ν_{SW} calculated through swelling experiments (ν_{SW} Zn@SiO_2/IR = 0.063 ± 0.005 mol kg^{-1}; ν_{SW} ZnO+SiO_2/IR = 0.032 ± 0.004 mol kg^{-1}).

The morphology of Zn@SiO_2/IR and ZnO+SiO_2/IR NCs after the vulcanization process, was studied by TEM. In both NCs, SiO_2 NPs appear dispersed within the rubber matrix, forming a quite continuous and homogeneous filler network composed by sub-micrometric aggregates (Figure 2a-b and Figure 2d-e).

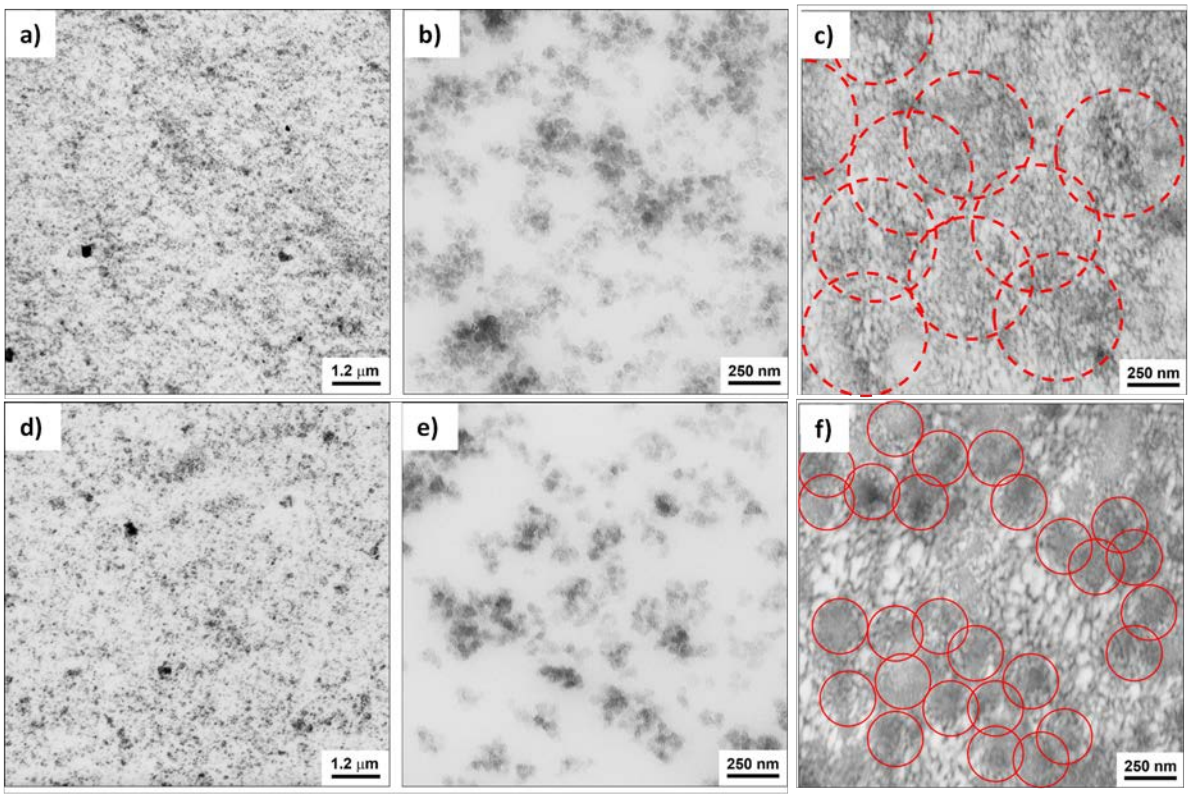

Figure 2. TEM images of: i) vulcanized pristine ZnO+SiO_2/IR (a,b) and Zn@SiO_2/IR (d,e) at two different magnifications; ii) vulcanized NCs after swelling and staining with OsO_4 vapors of ZnO+SiO_2/IR (c) and Zn@SiO_2/IR (f). Circles in c) and f) highlight the network domains.

Both samples were then prepared for NVTEM following the method proposed by Shiibashi et al. [33] (paragraph 2.3). NVTEM is based on the visualization of the interpenetrating polymer networks (IPNs), realized by swelling to equilibrium the rubber NCs with styrene and then polymerizing it into the pre-existent rubber network, thus resulting in a polystyrene (PS)-

rubber composite material [15,34]. A constrained phase separation occurs during styrene polymerization, resulting in a mesh structure comprising bundles of strained elastomeric chains. PS-swollen rubber samples embedded in the formed PS matrix were analyzed by TEM before and after being stained with OsO_4, which reacts with carbon-carbon double bonds present along the elastomer chains (but which does not react with the more stable benzene rings pendant from the PS backbone). Consequently, the unsaturated elastomer chains appear in TEM images darker than the non-stained saturated PS counterparts (white regions). As already observed in the literature [35], the distances between silica particles result enlarged after PS swelling (Figure S3). Instead, in both ZnO+SiO_2/IR and Zn@SiO_2/IR a pattern of cross-linked IR formed by dark lines meshes appears on the whole analyzed area after the selective staining of the unsaturated IR polymer chains (Figure 2c and 2f).

In ZnO+SiO_2/IR, the cross-links (dark zones) cover almost the whole NC specimen observed, and the cured mesh size is homogeneous in the entire NC (Figure 2c). The slightly darker zones seem to identify the formation of network domains at the micrometric scale (highlighted by the red dotted circles in Figure 2c) with a locally higher cross-link density. The presence of these domains is probably related to the local distribution of ZnO and curing agents, which promote the growth and propagation of cross-links in the vicinity of large activator ZnO particles, as already observed in the literature [22]. However, the partial overlapping of all network domains guarantees the formation of a quite homogeneous network, where silica filler particles and aggregates are difficult to be recognized as covered by the stained pattern.

On the contrary, a less homogeneous reticulated rubber pattern is evident in Zn@SiO_2/IR (Figure 2f), which shows darker zones surrounding the filler aggregates, as well as white areas of swollen polymer crossed by looser cross-linked chains without any filler aggregate. Besides, the mesh size of the rubber cross-link network looks appears smaller in the

surrounding of silica particles/aggregates and increases moving far away from them. The mesh sizes are strictly correlated to the cross-link density of the rubber, as the smaller the meshes, the higher the cross-link density of the elastomeric matrix. Thus, NVTEM observations indicate that in Zn@SiO_2/IR silica filler particles or aggregates are surrounded by a highly cured (stained) zone and that the highest curing density detected close to the silica surface progressively reduces moving to the bulk rubber matrix.

TD-NMR measurements were performed to study the rubber chains dynamics and to complement the morphological analysis of Zn@SiO_2/IR and ZnO+SiO_2/IR. First, ν_{NMR} was evaluated by MQ-NMR, by measuring the incomplete motional averaging of the dipolar interactions in terms of D_{res}, that is connected to the higher constraint on the motions of polymer chains due to cross-linking (Eqs. S3-S4). Figure 3a reports the normalized intensity of the reference (I_{ref}) and MQ build-up (I_{MQ}) signals on Zn@SiO_2/IR (data for ZnO+SiO_2/IR are reported in Figure S4), as well as the build-up recalculated after correction for slowly relaxing tails, that indicates the good fitting of the normalized data with the Tikhonov regularization using Abragam-like kernel function (red line in Figure 3a).

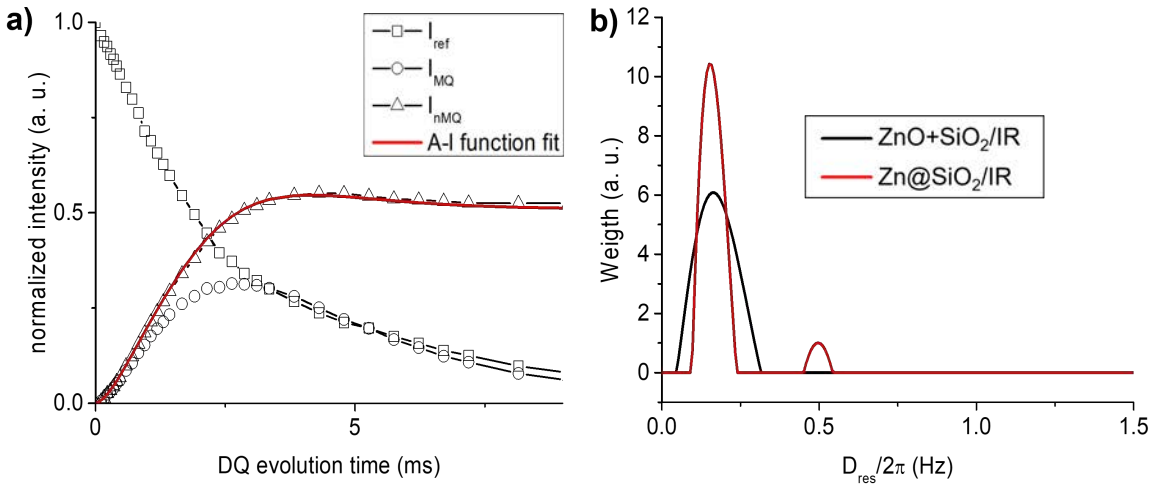

Figure 3. a) Reference (squares) and MQ (circles) intensities measured on Zn@SiO_2/IR; the resulting normalized intensity is shown with triangles, and the relevant fitting with Abragam-like functions is shown with

a solid red line; b) Distribution of D_{res} for ZnO+SiO_2/IR (black line) and Zn@SiO_2/IR (red line) samples are shown.

The resulting distribution of D_{res} (Figure 3b) show the presence of a bimodal distribution of Zn@SiO_2/IR, with a peak appearing at high D_{res} values that is absent in ZnO+SiO_2/IR. The integration of these peaks further suggests that the second component in Zn@SiO_2/IR could be connected to about 5% of the rubber mass. Despite MQ-NMR on itself provides no spatial resolution on the distribution of the regions with different mobility and network density, this behavior is consistent with the presence of regions with increased cross-linking than ZnO+SiO_2/IR.

From these data, the average D_{res} values is found equal to 169 ± 4 Hz and 190 ± 5 Hz, for ZnO+SiO_2/IR and Zn@SiO_2/IR respectively. For comparison, the sulfur vulcanized NR presented in previous works [30] had an average D_{res} of 165 Hz and was prepared with 1.3 phr sulfur at 150 °C, thus validating the herein used data elaboration. From D_{res}, the calculated ν_{NMR} is equal to 0.135 mol kg^{-1} and 0.152 mol kg^{-1} for ZnO+SiO_2/IR and Zn@SiO_2/IR, respectively. The higher values of ν_{NMR} calculated by MQ TD-NMR for both NCs compared to ν_{SW} from the equilibrium swelling are in agreement with the literature [29], as NMR measures both chemical cross-link restrictions and physical restrictions imposed by entanglements, that are instead partially released at equilibrium swelling state. Nevertheless, both NMR and swelling experiments evidence the highest cross-linking densities achieved in the presence of Zn@SiO_2/IR.

As a second step, the measurement of the rigid fraction of rubber was performed on both samples using the analysis of MSE refocused FID (Figure 4). In fact, by using Zn@SiO_2 a different interface between the surface of filler NPs and the rubber matrix can be expected compared to ZnO+SiO_2/IR, where bare SiO_2 NPs are compatibilized by adding TESPD

(paragraph 2.2). In the MSE experiment, the fraction indicated as "rigid" is endowed with an extremely limited mobility, such as in the crystal or glassy phase.

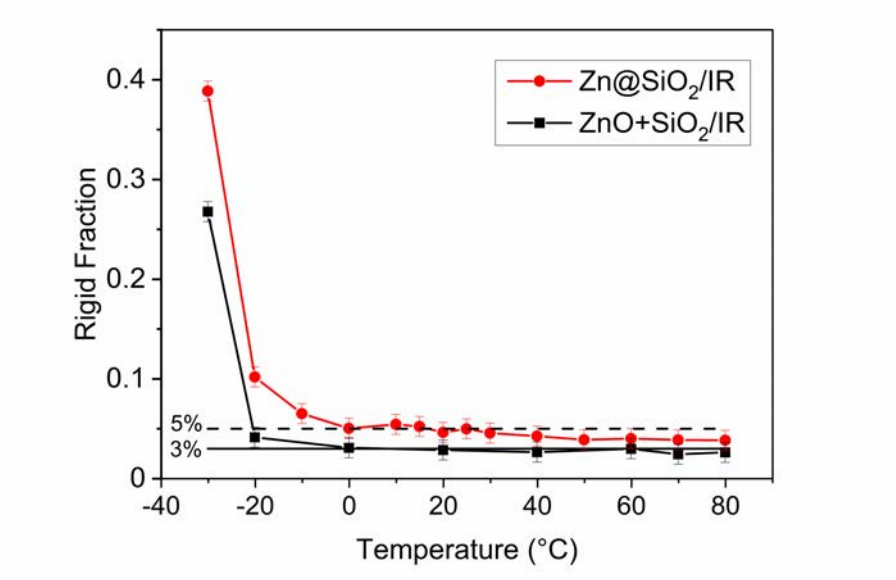

Figure 4. Rigid fraction measured by MSE-refocused TD-NMR as function of temperature. Based on triplicate measurements, a 1% error bar was inserted.

Experiments performed on Zn@SiO_2/IR and ZnO+SiO_2/IR indicate that the polymer chains are mostly mobile over -20 °C, whereas below that temperature there is a sharp increase of the rigid fraction, usually associated to the approach of the glass transition temperature (T_g). In fact, the rigid fraction detected by MSE-NMR typically endures few tens of degrees after the T_g [36], and indeed DSC measurements show that T_g of both NCs is about -50 °C (Figure S5).

Interestingly, at temperatures far above the T_g a fraction of polymer with extremely reduced mobility persists in both NCs, corresponding to about 3% of the total rubber mass for ZnO+SiO_2/IR in the temperature range 0-80 °C, and about 5% for Zn@SiO_2/IR, between 0-30 °C, that slowly decreases to about 4% at 60 °C. For ZnO+SiO_2/IR, this fixed amount is probably due to the polymer molecules tightly adsorbed on the surface of SiO_2 NPs mainly through silane compatibilizing agent TESPD. Instead, for Zn@SiO_2/IR, even if the Zn(II) complex on the SiO_2 surface may act as a compatibilizing agent, the evolution of rigid

fraction (with a gradient starting from T_g) is more consistent with the formation of an adsorbed layer of highly cured rubber starting from the surface of Zn@SiO_2 NPs [37]. The effects described above are close to the limits of precision of the MSE technique; however, they are consistently measured at any temperature, and even at 60 °C the difference between the FIDs is detectable (Figure S6).

Considering the different microstructural properties of Zn@SiO_2/IR and ZnO+SiO_2/IR, their mechanical behavior was investigated aiming at correlating the microscopic features to macroscopic behaviors. Figure 5 reports the DMA outputs, expressed as the storage modulus value E' plotted versus the applied static strain ε_s.

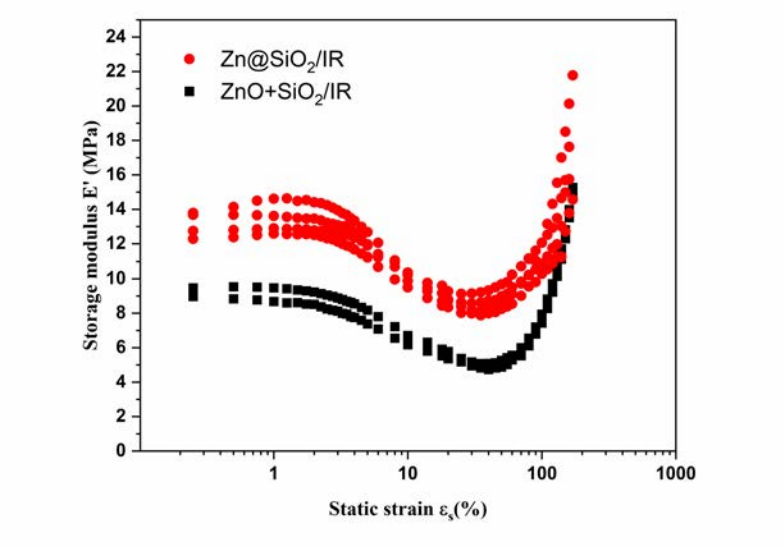

Figure 5. DMA results for Zn@SiO_2/IR (red curves) and ZnO+SiO_2/IR (black curves) NCs reported as the storage modulus E' vs static strain ε_s.

At low strains, E' decreases as ε_s increases, from a value referred to as $E'_{low\ strain}$ to a minimum value (E'_{min}) and then, at higher strains, it increases. E' trend can be correlated to NC structural features and strain induced rearrangements. The decrease of E' in the low strain range is due to dissipative rupture of filler-filler and filler-polymer interactions [38,39]. The strain level at which E' is minimum ($\varepsilon_{@E'min}$) can be somehow related to the maximum chain extensibility of the NC network.

It can be observed that (i) E' values are higher for Zn@SiO_2/IR than for ZnO+SiO_2/IR, in the whole strain range explored and (ii) the decrease of E' related to a strain increase ($\Delta E' = E'_{low\ strains} - E'_{min}$ as reported in Table 1), is larger for Zn@SiO_2/IR. These results suggest the structure of the two materials are somehow different, and a different mechanical response could be expected.

From the stress strain curves relevant to the uniaxial tensile tests, the Mooney Rivlin plots for the two rubber NCs were obtained (Figure 6**)**. The materials show a similar behavior, typical for reinforced rubbers [40]: at relatively low strains (corresponding to 1/λ values close to 1) material softening occurs, linked to the disruption of filler-filler and filler-rubber interactions. Whereas, at higher strains (corresponding to low 1/λ values) the reduced stress increases probably due to the limited polymer chain extensibility. Zn@SiO_2/IR NC shows higher values of the reduced stress σ* than ZnO+SiO_2/IR, indicating a higher stiffness, but it breaks at lower strains than ZnO+SiO_2/IR, suggesting a more brittle behavior. Besides, the strain at which the maximum extension of the polymer network is reached ($\varepsilon^*_{min} = \ln\lambda_{\sigma^*min}$) is lower for Zn@$SiO_2$/IR (56±5%) compared to ZnO+SiO_2/IR (75±6%). DMA and tensile tests results suggest a higher orientability of the polymer chains in Zn@SiO_2/IR, consistent with a different network structure and a higher cross-linking density.

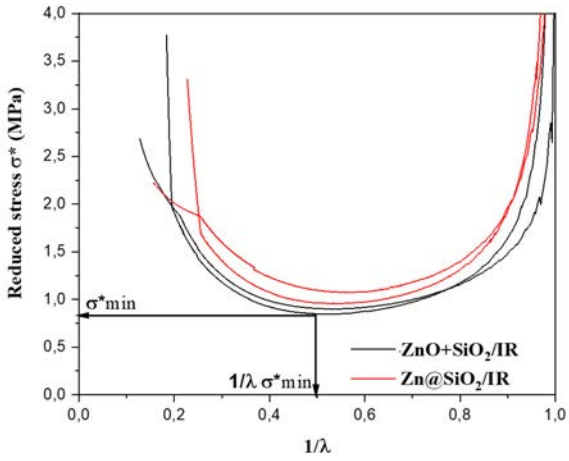

Figure 6. Mooney Rivlin plots for Zn@SiO_2/IR (red line) and ZnO+SiO_2/IR (black line) NCs.

Fracture tests on notched specimens were performed to evaluate the materials fracture toughness, which is affected by NCs micro-structure and testing conditions [41]. Figure 7 reproduces the video-recorded frames captures at the onset of the crack that, as expected, propagates perpendicularly to the loading direction (direction indicated by the two black arrows). As it typically occurs in the case of rubbery materials, the notch produced by the razor blade is largely blunted when the fracture is initiated. However, the blunting is greater for ZnO+SiO_2/IR (Figure 7a) than for Zn@SiO_2/IR (Figure 7b). This result indicates that higher strains are reached at fracture onset in ZnO+SiO_2/IR than in Zn@SiO_2/IR and it is related to the different fracture phenomenology observed in the two materials. As concerns ZnO+SiO_2/IR, a crack deviation takes place: two cracks, indicated by the white arrows in Figure 7a, initiate and propagate parallel to the loading direction, before the onset of the crack propagating perpendicularly to the loading direction takes place while no crack deviation occurs in Zn@SiO_2/IR.

Crack deviation is related to the capability of the polymer chains close to the tip of the notch to orient in the loading direction[40]. This capability is strongly related to the material structure and cross-linking degree [42] and it depends also on the loading conditions [41]. Crack deviation can be suppressed in highly cross-linked compounds or if the applied strain rate is too high, conditions that do not favor to reach the strength anisotropy required for crack deviation. In the case of Zn@SiO_2/IR, the higher cross-linking density promoted by the zinc centers at the surface of SiO_2 NPs does not favor crack deviation for the applied loading conditions. It must be taken into consideration that, as already observed, when crack deviation happens, much larger strain can be reached both at the notch tip and in the whole specimen. Thus, a larger energy dissipation occurs, and high fracture toughness values should be expected.

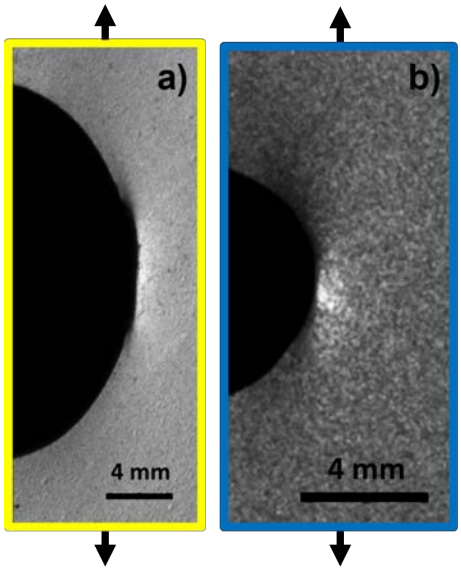

Figure 7. Videoframes recorded just before the forward crack onset for the a) ZnO+SiO_2/IR and b) Zn@SiO_2/IR NCs, respectively. The black arrows represent the loading direction while the white ones point the sideways cracks forming in ZnO+SiO_2/IR compound.

J integral was evaluated at fracture onset, (Jc in Table 1) as an index of material fracture toughness. The lower Jc of Zn@SiO_2/IR is consistent with the fracture phenomenology observed and the more brittle behavior compared to ZnO+SiO_2/IR is related to differences in their structure.

4. Discussion

The spatial distribution of the rubber cross-links in Zn@SiO_2/IR NC and ZnO+SiO_2/IR NCs was evaluated by their microstructural features from morphological TEM/NVTEM analysis and solid-state NMR techniques.

The main role of zinc in the activation of vulcanization reactions was confirmed and the cross-link formation was demonstrated to be influenced by the different morphology and composition of curing activators and by their local distribution within the rubber matrix. In fact, in ZnO+SiO_2/IR, ZnO activator promotes the growth of sulfur cross-links starting from the Zn(II) centers dispersed in the rubber matrix when released from ZnO particles after the interaction with curing agents. This is responsible for the formation of network domains into

the polymeric matrix, whose overlapping leads to the creation of a quite homogeneous structure of the polymer cross-links network, as observed by NVTEM. On the other side, in IR composite enclosing Zn@SiO_2 double function filler, the localization of Zn(II) centers anchored on the silica surface prompts the cross-link process in proximity to the SiO_2 NPs surface. The stable Zn-APTES bonds keep Zn(II) ions linked to SiO_2 and, at the same time, allow them to act as active centers able to form intermediate species (i.e., active sulfurating agents) by reacting with sulfur, accelerators and polymer. Consequently, the polymer chains cross-linking process originate from the silica particles and propagates towards the bulk polymer. Thus, the cross-link density of the polymer network gradually spreads from the surface of the SiO_2 filler, being highest close to the NPs.

This peculiar cross-links' distribution is confirmed also by MQ-NMR analysis since Zn@SiO_2/IR shows the presence of a bimodal network, whose components are assigned to i) the network of cross-linked polymer chains in the bulk rubber structure, also identified as single component in ZnO+SiO_2/IR and ii) about 5% of rubber with higher cross-link density, related to the higher cross-linked chains close to SiO_2 NPs. By approximating Zn@SiO_2/IR NC to an ideal dispersion of silica NPs within the rubber matrix and considering the specific surface area of Zn@SiO_2 (107 g m^{-2} by BET [27]), this portion corresponds approximately to a layer of 1 nm around each Zn@SiO_2 NPs with a higher cross-linking density than the bulk rubber matrix.

Besides, MSE-NMR analysis demonstrates that the different distribution of the cross-links in the rubber matrix modifies the mobility of the polymer chains at the interface with the filler particles. In ZnO+SiO_2/IR the interactions filler surface/rubber and the fraction of immobilized polymer are mainly determined by the compatibilizing agent TESPD able to react on the filler surface and to link the chains with poly-sulfide groups. On the other side, Zn@SiO_2/IR is characterized by a higher rigid fraction of rubber even in the absence of

compatibilizing agents as TESPD. Zinc single sites linked by APTES on the silica surface in Zn@SiO_2 may act themselves as compatibilizing agent. However, the presence of a strongly immobilized rubber layer is more consistent with the adsorption of highly cured rubber very close to the surface of silica.

The different cross-links' distribution of the two NCs, arising from the different structure of the zinc activator, is responsible for their non-equivalent mechanical behaviors, thus affecting the macroscopic response of the NCs materials. The higher cross-linking density of Zn@SiO_2/IR NC was consistent with the higher $\varepsilon@E'_{min}$ measured by tensile tests (Figure 6) and the increase of E' in the DMA tests in the whole strain range explored (Figure 5) that led to a higher stiffness of the material. Besides, the reduction of $\varepsilon@E'_{min}$ in Zn@SiO_2/IR compared to ZnO+SiO_2/IR (Table 1), evidenced a lower extensibility of the network in Zn@SiO_2/IR and a more easily orientation of the polymer chains.

Finally, also the different fracture phenomenology is a strong indication of the differently cross-linked structures formed during the curing process: in fact, crack deviation occurs because of strength anisotropy at the crack tip, arising from the ability of the filled rubber network to be oriented in the loading direction. In the high cross-linked matrix of Zn@SiO_2/IR NC both the different spatial distribution and the higher density of crosslinks hinder the molecular orientation of the polymer chains at the tip of the crack, so the fracture occurs through the onset of a crack propagating along the original notch.

5. Conclusions

This work demonstrated that the localization of the vulcanization reaction in SiO_2 filled IR NCs provides a change in the microscopic structure of the cross-linked rubber network and, consequently, led to different mechanical behaviors, achieving a fine control of micro- and macro-properties of the rubber products. Besides, the localization and spatial distribution of the cross-link formation was demonstrated to be influenced by the different morphology of

zinc-based curing activators and by their relative arrangements close to the filler NPs.

In fact, in ZnO+SiO_2/IR NCs, vulcanized with m-ZnO as activator, a quite homogeneous structure of the polymer cross-links network is the result of the overlapping of large network domains, promoted by ZnO dispersed in the rubber matrix. On the contrary, in Zn@SiO_2/IR NCs, the Zn(II) single sites anchored on SiO_2 prompts the cross-link process in proximity to the SiO_2 NPs surface. Thus, the highest cross-link density of the rubber network is localized close to the SiO_2 NPs and gradually spreads from their surface to the bulk, showing a higher amount of a strongly immobilized rubber layer at the fille rubber interface compared to ZnO+SiO_2/IR.

The different cross-links' localization is responsible for the non-equivalent mechanical response of ZnO+SiO_2/IR and Zn@SiO_2/IR NCs at small strains and at fracture. Zn@SiO_2/IR material resulted to have higher stiffness but lower extensibility of the network and more easily orientation of the polymer chains compared to ZnO+SiO_2/IR; besides it shows lower fracture toughness without crack deviations, strong indications of the highest and more localized cross-linking density.

All the results highlight the existence of a strong correlation between the composites structural features and their macroscopic behavior, paving the way to the possibility of modulating the mechanical properties of final materials for different applications through the localization of the cross-linking network by tuning the nature of the curing agents.

Acknowledgements

This work was in the frame of the "International Doctoral School in Functional Materials for Research and Innovation" program and of the EU upscaling project SAFE-VULCA (reference number 18145, 2019-2021) funded by the European Institute of Innovation and Technology (EIT) Raw Materials, a body of the European Commission, under the Horizon 2020, the EU Framework Program for Research and Innovation. S.M. and P.M. thank the

CORIMAV (Consortium for the Research of Advanced Materials between Pirelli and University of Milano Bicocca) for its support within the PCAM European Doctoral Program.

References

[1] J.B. Donnet, E. Custodero, Reinforcement of Elastomers by Particulate Fillers, Sci. Technol. Rubber. (2005) 367–400. https://doi.org/10.1016/B978-012464786-2/50011-0.

[2] R. Scotti, M. D'Arienzo, B. Di Credico, L. Giannini, F. Morazzoni, Silica-Polymer Interface and Mechanical Reinforcement in Rubber Nanocomposites, in: Hybrid Org. Interfaces Towar. Advanded Funct. Mater., 2018: pp. 151–198. https://doi.org/10.1002/9783527807130.ch4.

[3] K. Sahakaro, Mechanism of reinforcement using nanofillers in rubber nanocomposites, Elsevier Ltd, 2017. https://doi.org/10.1016/B978-0-08-100409-8.00003-6.

[4] A.Y. Coran, Vulcanization, in: E.R. Eirich (Ed.), Sci. Technol. Rubber, Ed. Academic Press, San Diego, 1978: p. 291.

[5] M.M. Coleman, J.R. Shelton, J.L. Koenig, Sulfur Vulcanization of Hydrocarbon Diene Elastomers, Ind. Eng. Chem. Prod. Res. Dev. 13 (1974) 154–166. https://doi.org/10.1021/i360051a002.

[6] P. Ghosh, S. Katare, P. Patkar, E. Al., Sulfur vulcanization of natural rubber for benzothiazole accelerated formulations : From reaction mechanisms to a rational kinetic model, Rubber Chem. Technol. 76 (2003) 592–693.

[7] M.R. Krejsa, J.L. Koenig, A review of sulfur crosslinking fundamentals for accelerated and unaccelerated vulcanization, Rubber Chem. Technol. 66 (1993) 376–410.

[8] N.J. Morrison, M. Porter, Temperature Effects on the Stability of Intermediates and Crosslinks in Sulfur Vulcanization, Rubber Chem. Technol. 57 (1984) 63–85.

[9] G. Heideman, R.N. Datta, J.W.M. Noordermeer, B. van Baarle, Activators in Accelerated Sulfur Vulcanization, Rubber Chem. Technol. 77 (2004) 512–541. https://doi.org/10.5254/1.3547834.

[10] A. V. Chapman, The influence of excess zinc stearate on the chemistry of sulphur vulcanization of natural rubber, Phosphorus. Sulfur. Silicon Relat. Elem. 59 (1991) 271–274. https://doi.org/10.1080/10426509108045740.

[11] G. Heideman, J.W.M. Noordermeer, R.N. Datta, B. Van Baarle, Various ways to reduce zinc oxide levels in S-SBR rubber compounds, Macromol. Symp. 245–246 (2006) 657–667. https://doi.org/10.1002/masy.200651393.

[12] P.J. Nieuwenhuizen, S. Timal, J.M. Van Veen, Homogeneous Zinc(II) catalysis in accelerated vulcanization. I. Reaction-stge modeling and cross-link formation, Rubber Chem. Technol. 71 (1998) 751–765.

[13] M. D'Arienzo, S. Mostoni, R. Crapanzano, C. Cepek, B. Di Credico, M. Fasoli, S. Polizzi, A.

Vedda, I. Villa, R. Scotti, Insight into the Influence of ZnO Defectivity on the Catalytic Generation of Environmentally Persistent Free Radicals in ZnO/SiO<inf>2</inf> Systems, J. Phys. Chem. C. 123 (2019). https://doi.org/10.1021/acs.jpcc.9b06900.

[14] P. Versloot, J.G. Haasnoot, P.J. Nieuwenhuizen, J. Reedijk, M. van Duin, J. Put, Sulfur Vulcanization of Simple Model Olefins, Part V: Double Bond Isomerization during Accelerated Sulfur Vulcanization as Studied by Model Olefins, Rubber Chem. Technol. 70 (2011) 106–119. https://doi.org/10.5254/1.3538411.

[15] A.V. Chapman, A.J. Tinker, Vulcanization of blends - crosslink distribution and its effect on properties, KGK Kautschuk Gummi Kunststoffe. 10 (2003) 533–544.

[16] F. Ignatz-Hoover, B.H. To, R.N. Datta, A.J. De Hoog, N.M. Huntink, A.G. Talma, Chemical Additives Migration in Rubber, Rubber Chem. Technol. 76 (2011) 747–768. https://doi.org/10.5254/1.3547765.

[17] D.A. Lederer, K.E. Kear, G.H. Kuhls, Diffusion of curatives. I, Rubber Chem. Technol. 55 (1982) 1482–1498. https://meridian.allenpress.com/rct.

[18] H. Dohi, S. Horiuchi, Heterogeneity of a vulcanized rubber by the formation of ZnS clusters, Polymer (Guildf). 48 (2007) 2526–2530. https://doi.org/10.1016/j.polymer.2007.03.004.

[19] M.A. Rana, J.L. Koenig, Observation of Spatial Inhomogeneities in N-tert-Butylbenzothiazolesulfenamide–Sulfur Cured High-Vinyl Polybutadiene Using NMR Imaging, Macromolecules. 27 (1994) 3727–3734. https://doi.org/10.1021/ma00092a008.

[20] M. Hernández, J.L. Valentín, M.A. López-Manchado, T.A. Ezquerra, Influence of the vulcanization system on the dynamics and structure of natural rubber: Comparative study by means of broadband dielectric spectroscopy and solid-state NMR spectroscopy, Eur. Polym. J. 68 (2015) 90–103. https://doi.org/10.1016/j.eurpolymj.2015.04.021.

[21] M.A. Mansilla, J.L. Valentín, M.A. López-Manchado, A. González-Jiménez, A.J. Marzocca, Effect of entanglements in the microstructure of cured NR/SBR blends prepared by solution and mixing in a two-roll mill, Eur. Polym. J. 81 (2016) 365–375. https://doi.org/10.1016/j.eurpolymj.2016.06.023.

[22] Y. Ikeda, N. Higashitani, K. Hijikata, Y. Kokubo, Y. Morita, M. Shibayama, N. Osaka, T. Suzuki, H. Endo, S. Kohjiya, Vulcanization: New focus on a traditional technology by small-angle neutron scattering, Macromolecules. 42 (2009) 2741–2748. https://doi.org/10.1021/ma802730z.

[23] T. Ohashi, T. Sato, T. Nakajima, P. Junkong, Y. Ikeda, Necessity of two-dimensional visualization of validity in the nanomechanical mapping of atomic force microscopy for sulphur cross-linked rubber, RSC Adv. 8 (2018) 32930–32941. https://doi.org/10.1039/c8ra06669h.

[24] K. Miyaji, T. Sugiyama, T. Ohashi, K. Saalwächter, Y. Ikeda, Study on Homogeneity in Sulfur Cross-Linked Network Structures of Isoprene Rubber by TD-NMR and AFM - Zinc Stearate

System, Macromolecules. 53 (2020) 8438–8449. https://doi.org/10.1021/acs.macromol.0c01266.

[25] J.L. Valentín, P. Posadas, A. Fernández-Torres, M.A. Malmierca, L. González, W. Chassé, K. Saalwächter, Inhomogeneities and chain dynamics in diene rubbers vulcanized with different cure systems, Macromolecules. 43 (2010) 4210–4222. https://doi.org/10.1021/ma1003437.

[26] A.J. Tinker, Distribution of crosslinks in vulcanized blends, Rubber Chem. Technol. 68 (1995) 461–481.

[27] S. Mostoni, M. D'Arienzo, B. Di Credico, L. Armelao, M. Rancan, S. Dirè, E. Callone, R. Donetti, A. Susanna, R. Scotti, Design of a Zn Single-Site Curing Activator for a More Sustainable Sulfur Cross-Link Formation in Rubber, Ind. Eng. Chem. Res. 60 (2021) 10180–10192. https://doi.org/10.1021/acs.iecr.1c01580.

[28] a. Susanna, L. Armelao, E. Callone, S. Dirè, M. D'Arienzo, B. Di Credico, L. Giannini, T. Hanel, F. Morazzoni, R. Scotti, ZnO nanoparticles anchored to silica filler. A curing accelerator for isoprene rubber composites, Chem. Eng. J. 275 (2015) 245–252. https://doi.org/10.1016/j.cej.2015.04.017.

[29] M.K. Dibbanti, M. Mauri, L. Mauri, G. Medaglia, R. Simonutti, Probing small network differences in sulfur-cured rubber compounds by combining nuclear magnetic resonance and swelling methods, J. Appl. Polym. Sci. 132 (2015) 1–8. https://doi.org/10.1002/app.42700.

[30] W. Chassé, J.L. Valentn, G.D. Genesky, C. Cohen, K. Saalwächter, Precise dipolar coupling constant distribution analysis in proton multiple-quantum NMR of elastomers, J. Chem. Phys. 134 (2011). https://doi.org/10.1063/1.3534856.

[31] M. Mauri, M.K. Dibbanti, M. Calzavara, L. Mauri, R. Simonutti, V. Causin, Time domain nuclear magnetic resonance: A key complementary technique for the forensic differentiation of foam traces, Anal. Methods. 5 (2013) 4336–4344. https://doi.org/10.1039/c3ay40330k.

[32] B.H. Kim, C.R. Joe, Single Specimen Test Method for Determining Frecture Energy (Jc) of Highly Deformable Materials, Eng. Fract. Mech. 32 (1989) 155–161.

[33] T. Shiibashi, K. Hirose, N. Tagata, Gel structures of natural rubber and synthetic isoprene rubber, Kobunshi Ronbunshu. 46 (1989) 465–472.

[34] H.L. Frisch, Y. Xue, Visualization of network structure in poly(butadiene)/polystyrene pseudo interpenetrating polymer networks by transmission electron microscopy, Polym. J. 26 (1994) 828–832. https://doi.org/10.1295/polymj.26.828.

[35] S.S. Sarkawi, W.K. Dierkes, J.W.M. Noordermeer, Elucidation of filler-to-filler and filler-to-rubber interactions in silica-reinforced natural rubber by TEM Network Visualization, Eur. Polym. J. 54 (2014) 118–127. https://doi.org/10.1016/j.eurpolymj.2014.02.015.

[36] S. Bonetti, M. Farina, M. Mauri, K. Koynov, H.J. Butt, M. Kappl, R. Simonutti, Core@shell Poly(n-butylacrylate)@polystyrene Nanoparticles: Baroplastic Force-Responsiveness in Presence of Strong Phase Separation, Macromol. Rapid Commun. 37 (2016) 584–589.

https://doi.org/10.1002/marc.201500625.

[37] A.M. Mayes, Glass Transition of Amorphous Polymer Surfaces, Macromolecules. 27 (1994) 3114–3115. https://doi.org/10.1021/ma00089a033.

[38] E. Cazzoni, R. Calabrò, C. Marano, M. Rink, G. Barbaglia, Mechanical characterization of carbon black filled NR/BR compounds from small strains up to fracture, in: Const. Model. Rubber VIII, 2013: p. 329.

[39] W. Luo, X. Hu, C. Wang, Q. Li, Frequency- and strain-amplitude-dependent dynamical mechanical properties and hysteresis loss of CB-filled vulcanized natural rubber, Int. J. Mech. Sci. 52 (2010) 168–174. https://doi.org/10.1016/j.ijmecsci.2009.09.001.

[40] M.C. Boyce, E.M. Arruda, Constitutive models of rubber elasticity: a review, Rubber Chem. Technol. 73 (2000) 504–523.

[41] M. Boggio, C. Marano, M. Rink, Time-dependence of fracture behaviour of carbon black filled natural rubber, Const. Model. Rubber VIII. 7 (2011).

[42] C. Marano, M. Boggio, E. Cazzoni, M. Rink, Fracture phenomenology and toughness of filled natural rubber compounds via the pure shear test specimen, Rubber Chem. Technol. 87 (2014) 501–515. https://doi.org/10.5254/rct.14.86950.

Tables

Table 1. Storage modulus value at low strains ($E'_{low\ strains}$) and its minimum value (E'_{min}) measured at $\varepsilon@E'_{min}$ for the two rubber NCs; $\Delta E'$ is a measure of the strain dependency of the material rigidity. In the last column: toughness J_C values of IR NCs from fracture tests.

Sample	**$E'_{low\ strains}$ (MPa)**	**E'_{min} (MPa)**	**$\varepsilon@E'_{min}$ (mm/mm)**	**$\Delta E'$**	**J_C (kJ m^{-2})**
ZnO+SiO_2/IR	9.3	4.9	0.4	4.4	9 ± 4
Zn@SiO_2/IR	14.6	8.2	0.35	6.4	30 ± 10